Induced pluripotent stem cells used to reveal drug actions in a long QT syndrome family with complex genetics

Cecile Terrenoire,[1] Kai Wang,[1] Kelvin W. Chan Tung,[4] Wendy K. Chung,[2,3] Robert H. Pass,[6] Jonathan T. Lu,[2] Jyh-Chang Jean,[5] Amel Omari,[5] Kevin J. Sampson,[1] Darrell N. Kotton,[5] Gordon Keller,[4] and Robert S. Kass[1]

[1]Department of Pharmacology, [2]Department of Medicine, and [3]Department of Pediatrics, College of Physicians and Surgeons, Columbia University Medical Center, New York, NY 10032
[4]McEwen Centre for Regenerative Medicine, University Health Network, Toronto, Ontario M5G 1L7, Canada
[5]Center for Regenerative Medicine, Boston University and Boston Medical Center, Boston, MA 02118
[6]Department of Pediatrics, Albert Einstein College of Medicine, The Children's Hospital at Montefiore, Bronx, NY 10467

Understanding the basis for differential responses to drug therapies remains a challenge despite advances in genetics and genomics. Induced pluripotent stem cells (iPSCs) offer an unprecedented opportunity to investigate the pharmacology of disease processes in therapeutically and genetically relevant primary cell types in vitro and to interweave clinical and basic molecular data. We report here the derivation of iPSCs from a long QT syndrome patient with complex genetics. The proband was found to have a de novo *SCN5A* LQT-3 mutation (F1473C) and a polymorphism (K897T) in *KCNH2*, the gene for LQT-2. Analysis of the biophysics and molecular pharmacology of ion channels expressed in cardiomyocytes (CMs) differentiated from these iPSCs (iPSC-CMs) demonstrates a primary LQT-3 (Na^+ channel) defect responsible for the arrhythmias not influenced by the *KCNH2* polymorphism. The F1473C mutation occurs in the channel inactivation gate and enhances late Na^+ channel current (I_{NaL}) that is carried by channels that fail to inactivate completely and conduct increased inward current during prolonged depolarization, resulting in delayed repolarization, a prolonged QT interval, and increased risk of fatal arrhythmia. We find a very pronounced rate dependence of I_{NaL} such that increasing the pacing rate markedly reduces I_{NaL} and, in addition, increases its inhibition by the Na^+ channel blocker mexiletine. These rate-dependent properties and drug interactions, unique to the proband's iPSC-CMs, correlate with improved management of arrhythmias in the patient and provide support for this approach in developing patient-specific clinical regimens.

INTRODUCTION

Cardiomyocytes (CMs) differentiated from patient-specific induced pluripotent stem cells (iPSCs [iPSC-CMs]) have now been shown to provide valuable models of heritable cardiac arrhythmias, including catecholaminergic polymorphic ventricular tachycardia (Jung et al., 2012; Novak et al., 2012) and the congenital long QT syndrome (LQTS; Moretti et al., 2010; Itzhaki et al., 2011; Kamp, 2011; Masuda and Hanazono, 2011; Yazawa et al., 2011), diseases caused by mutations in genes coding for ion channels or ion channel–associated proteins. LQTS is a channelopathy now known to be caused by mutations in at least 12 different genes for which heterologous expression has revealed therapeutic strategies based on gene- and mutation-specific drug selection (Kass and Moss, 2006; Sauer et al., 2007; Ruan et al., 2009), and these strategies have begun to fulfill the promise of personalized disease management (Schwartz et al., 1995; An et al., 1996; Moss and Kass, 2005). However, particularly in the case of LQTS, patients with multiple mutations have more severe clinical phenotypes and may respond uniquely to pharmacologic therapies (Westenskow et al., 2004; Itoh et al., 2010; Zhang et al., 2012). In addition, there can be significant clinical variability between individuals with the same LQT mutation, possibly as a result of genetic modifiers. Patient-specific iPSC-CMs represent a platform with potential for investigating the molecular pharmacology of ion channel mutations expressed in these complex genetic backgrounds (Tiscornia et al., 2011; Gnecchi and Schwartz, 2012; Zhang et al., 2012) and may provide unique insight into therapeutic approaches for disease management.

In this study, we report generation of iPSC-CMs from each member of an LQTS-3 (LQT-3) family and the investigation of the molecular pharmacology of key ion channels. The proband had been found to have a

C. Terrenoire and K. Wang contributed equally to this paper.
Correspondence to Robert S. Kass: rsk20@columbia.edu

Abbreviations used in this paper: bFGF, basic fibroblast growth factor; bpm, beats per minute; CM, cardiomyocyte; DMEM, Dulbecco's modified Eagle's medium; hESC, human embryonic stem cell; ICD, implantable cardioverter defibrillator; iPSC, induced pluripotent stem cell; LQTS, long QT syndrome; MEF, mouse embryonic fibroblast; TTX, tetrodotoxin.

The Rockefeller University Press $30.00
J. Gen. Physiol. Vol. 141 No. 1 61–72
www.jgp.org/cgi/doi/10.1085/jgp.201210899

de novo mutation in the principal heart sodium channel (*SCN5A*) and a common polymorphism in *KCNH2* that codes for hERG, a critical heart potassium channel known to contribute to most cases of drug-induced LQTS (Mitcheson et al., 2000). In a first study, we had characterized the biophysical properties of the mutant sodium channels alone expressed in HEK293 cells and found that the mutation resulted in defects in inactivation consistent with the LQT phenotype observed in the proband (Bankston et al., 2007b). However, this study did not explain why the proband was resistant to drug therapy, and it did not investigate whether the hERG polymorphism played a role in the observed phenotype or in the response to drug therapy, nor did it report the function of the mutant sodium channel expressed in a cardiac cellular background genetically identical to that of the mutation carrier. Consequently, here we use iPSC-CMs to carry out a more complete study of the mutant sodium channel and hERG polymorphism in CMs derived from the proband's skin cells. Our studies demonstrate a primary LQT-3 (Na^+ channel) defect not influenced by the *KCNH2* polymorphism and drug interactions unique to the proband that correlate with improved management of arrhythmias in the patient and provide support for this approach in developing patient-specific clinical regimens.

MATERIALS AND METHODS

Human fibroblast reprogramming and characterization of iPSCs

Reprogramming was performed with the hSTEMCCA-loxPlentiviral vector, encoding the four human factors, OCT4, KLF4, SOX2, and cMYC, as previously described (Sommer et al., 2009; Somers et al., 2010; Wang et al., 2011). In brief, 10^5 human dermal fibroblasts were plated in Dulbecco's modified Eagle's medium (DMEM) with 10% FBS on a gelatin-coated 35-mm plastic tissue culture dish. The next day, 5 µg/ml polybrene was added to the media, and cells were infected with hSTEMCCA-loxPlentiviruses at a multiplicity of infection of 1. On day 2, the media was changed to serum-free iPSC media (see next section), and on day 6 cells were trypsinized and plated onto 10-cm gelatin-coated culture dishes that had been preseeded the day before with mitomycin C–inactivated mouse embryonic fibroblast (MEF) feeder cells. iPSC colonies were mechanically isolated 30 d after infection and expanded on MEF feeders in iPSC media. Dermal fibroblast reprogramming efficiency obtained with hSTEMCCA-loxP vector at a multiplicity of infection of 1 reached ∼1% (calculated by dividing the number of total colonies obtained on day 30 by the number of starting input fibroblasts).

Candidate iPSC clones were characterized by karyotype assay (G banding analysis), teratoma assay, and immunostaining. For teratoma formation assays, iPSC colonies were harvested with collagenase IV and resuspended in 140 ml DMEM/F12. 60 ml matrigel (BD) was added to the cell suspension at 4°C immediately before subdermal injection between the scapulae of an anesthetized severe combined immune deficiency/Beige mouse (strain 250; Charles River). Resulting tumors were harvested at 6–8 wk after injection and fixed in 4% paraformaldehyde, and paraffin tissue sections were prepared and stained with hematoxylin and eosin according to standard methods. For immunostaining assay, iPSC colonies were fixed with 4% paraformaldehyde and stained with mouse primary antibodies against SSEA-1, SSEA-4, TRA1-60, and TRA1-81 (ES Cell Characterization kit; EMD Millipore). Secondary Alexa Fluor 488–conjugated goat anti–mouse IgG or IgM (Invitrogen) was used for detection. For each individual, several iPSC clones were used in this study: proband, OA6 9, OA6 9Cr8, OA6 17Cr8, and OA6 22Cr8; father, HR-I-2R 2Cr, HR-I-7, and HR-I-15; and mother, HR-II-5 and HR-II-9.

iPSC culture and cardiac differentiation

iPSCs were maintained on irradiated MEFs in iPSC media consisting of DMEM/F12 (50:50; Corning) media with 20% serum replacement, 2 mM L-glutamine, 100 µM of nonessential amino acids, 50 U/ml penicillin, 50 µg/ml streptomycin (Invitrogen), 0.1 mM β-mercaptoethanol (Sigma-Aldrich), and 10 ng/ml human basic fibroblast growth factor (bFGF) as previously described (Kennedy et al., 2007; Kattman et al., 2011). 1 d before differentiation, iPSCs were feeder depleted by culture on matrigel in the aforementioned culture media. To induce differentiation, feeder-depleted cells were dissociated with 1 mg/ml collagenase B (Roche) for 20 min followed by TrypLE Express (Invitrogen) for 1 min. Cells were then plated as small clusters in a base media consisting of StemPro34 (Invitrogen) containing penicillin/streptomycin, 2 mM L-glutamine, 50 µg/ml ascorbic acid, 0.4 mM monothioglycerol (Sigma-Aldrich), and 1 ng/ml human BMP4 for 1 d to promote embryoid body formation. Embryoid bodies were cultured in the presence of human activin A and human BMP4 in StemPro34 base media to induce cardiac mesoderm, defined by coexpression of KDR and PDGFR-α (Kattman et al., 2011). Concentrations of BMP4 and activin A were optimized for the different iPSC clones, and 10 µM Rock inhibitor (Toronto Research Chemicals) was added at the aggregation and induction steps. $KDR^+PDGFR\text{-}\alpha^+$ mesoderm typically emerged between days 4 and 5 of differentiation. 1 d before measuring mesoderm development (day 3 or 4, depending on the cell line), BMP4 and activin A were removed and replaced with inhibitors of the Wnt (DKK1), activin/nodal/TGF-β (5.4 µM SB-431542; Cayman Chemical Co.), and bone morphogenetic protein (BMP; 1 µM dorsomorphin; Sigma-Aldrich) pathways for 2 d. At this stage, the inhibitors were removed, and the embryoid bodies were maintained in StemPro34 base media supplemented with human vascular endothelial growth factor and human bFGF until day 20. All differentiated populations (day 20) were monitored for expression of cardiac troponin T by intracellular flow cytometry to determine the proportion of CMs in each. Human BMP4, human activin A, human bFGF, human DKK1, and human vascular endothelial growth factor were purchased from R&D Systems.

Genomic sequencing

To confirm the presence of the genomic variants in the *SCN5A* and *KCNH2* genes in iPSCs, genomic DNA was extracted from iPSCs derived from each of the LQT-3 family members using the DNeasy Blood and Tissue kit (QIAGEN). PCR reactions to amplify the region of interest for sequencing consisted of 25-µl reaction volumes comprised of 100 ng genomic DNA, 1× reaction buffer, 1.5 µM $MgCl_2$, 0.25 mM deoxyribonucleotide triphosphate mixture, 5 µM of forward and reverse primers, and 1 U Taq polymerase. Primer sequences were as follows: SCN5A F1473 F, 5′-ATGGACACCCCTAGACAGCCCTCT-3′; SCN5A F1473 R, 5′-TGAGATGGGACCTGGAGCCTGAGT-3′; KCNH2 K897 F, 5′-GTGGGGCAGGAGAGCACTGAAA-3′; and KCNH2 K897 R, 5′-GATGGGCAGCATCTGGACAGCT-3′.

All thermocycling was performed with denaturation at 94°C for 5 min, 37 cycles of denaturation at 94°C for 30 s, annealing at 60°C for 30 s and extension at 72°C for 30 s, and a final extension step at 72°C for 7 min. PCR products were purified after

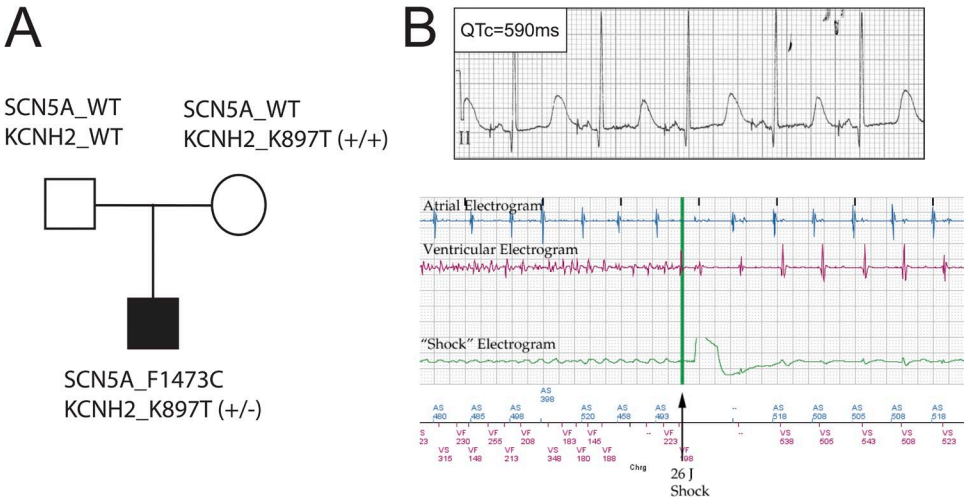

Figure 1. Clinical and genetic profile of the LQTS family. (A) Genotype of *SCN5A* and *KCNH2* of each family member. SCN5A_1473F/F is referred to as WT SCN5A in the text. See text (Results section hERG channel activity in iPSC-CMs) for definitions of *KCNH2* variants. (B, top) Surface electrocardiography lead II recorded from the LQT-3 proband before this study. QTc, QT interval corrected for heart rate. (bottom) Example of ICD detection and termination of ventricular tachyarrhythmia in proband.

electrophoresis through a 2% agarose gel using the Qiaquick DNA purification columns (QIAGEN) and were sequenced bidirectionally using the PCR primers (Genewiz).

CM dissociation

Beating embryoid bodies from 25 to 45 d after differentiation were dissociated for ∼30 min at 37°C in the presence of 200 U/ml collagenase II (Gibco) and 0.2 U/ml protease XIV (Sigma-Aldrich) in a solution containing 120 mM NaCl, 5.4 mM KCl, 5 mM $MgSO_4$, 5 mM Na-pyruvate, 20 mM glucose, 20 mM taurine, and 10 mM HEPES, pH 6.9. Isolated cells were then incubated at room temperature for 30 min in Kraft-Bruhe solution containing 85 mM KCl, 30 mM K_2HPO_4, 5 mM $MgSO_4$, 1 mM EGTA, 2 mM Na_2-ATP, 5 mM Na-pyruvate, 5 mM creatine, 20 mM taurine, and 20 mM glucose, pH 7.2. Cells were finally resuspended in DMEM supplemented with 10% FBS, 1 mM Na-pyruvate, 50 U/ml penicillin, 50 µg/ml streptomycin, and 2 mM L-glutamine and plated on 0.1% gelatin-coated 35-mm plastic Petri dishes. Isolated CMs were identified the next day by spontaneous contraction at ∼37°C, individually marked with an object marker (Nikon), and used for patch-clamp recordings within 48 h after plating.

Single-cell electrophysiology

For each individual, CMs derived from several iPSC clones were used for single-cell electrophysiological studies (see section Human fibroblast reprogramming . . .). These CMs (iPSC-CMs) were placed on the stage of an inverted microscope (Nikon), and patch-clamp experiments were performed at room temperature (23–25°C) using the whole-cell configuration with Axopatch 200B amplifiers (Axon Instruments).

Current clamp was conducted in previously described internal and external solutions (Terrenoire et al., 2005; Wang et al., 2011). Action potentials were triggered at 0.2 Hz by 3 ms of suprathreshold stimuli. Sodium current (I_{Na}), measured as tetrodotoxin (TTX; 50 µM)-sensitive current, was recorded with a previously described internal recording solution (Bankston et al., 2007b) and the following external solution: 130 mM NaCl, 5 mM CsCl, 2 mM $CaCl_2$, 1.2 mM $MgCl_2$, 0.05 mM $NiSO_4$, 10 mM HEPES, 5 mM glucose, pH 7.4, and 1 µM isradipine. I_{Na} late current (I_{NaL}) was measured as the TTX (50 µM)-sensitive current measured at 100 ms during depolarization to −10 mV from a −90-mV holding potential. I_{NaL} was normalized to peak TTX-sensitive I_{Na} ($I_{Na\ peak}$) measured at −10 mV and expressed as a percentage of peak current in relevant figures. Steady-state activation was studied by measuring the peak sodium conductance (G_{Na}) during a 100-ms test pulse to various test potentials from a −90-mV holding potential. Currents were normalized to currents measured at 20 mV, plotted against conditioning pulse voltage, and fitted with a Boltzmann equation to determine the channel midpoint of activation ($V_{1/2}$). The voltage dependence of I_{Na} inactivation was determined by measuring the peak current at −10 mV after application of conditioning pulses (from −130 to −20 mV for 500 ms) at 0.2 Hz. Currents were normalized to currents measured after the −130-mV conditioning pulse, plotted against conditioning pulse voltage, and fitted with a Boltzmann equation to determine the channel midpoint of inactivation ($V_{1/2}$). Recovery from inactivation was determined by measuring current at −10 mV after application of 50-ms conditioning pulses at −10 mV with interpulse intervals at −90 mV ranging from 0.1 to 1,500 ms. The potassium current I_{Kr}, measured as an E4031 (5 µM)-sensitive and chromanol 293B (30 µM)–insensitive current, was recorded using previously described internal and external (Terrenoire et al., 2005; Wang et al., 2011) solutions. To measure the voltage dependence of I_{Kr} activation, cells were depolarized from −40 to 50 mV (in 10-mV increments) for 2 s and then repolarized to −40 mV for 2 s at a pulse frequency of 0.1 Hz. Maximum tail current amplitudes were measured during this repolarizing pulse and plotted against the test pulse voltage. Activation curves (2-s isochronal), determined from amplitudes of deactivating current tails normalized to maximum tail current plotted against test pulse voltage, were fitted with a Boltzmann equation to determine the midpoint of activation ($V_{1/2}$). All reagents were purchased from Sigma-Aldrich unless otherwise specified.

Data analysis

Patch-clamp data were acquired with pClamp 8.2 (Axon Instruments) and analyzed with Origin 7.0 (OriginLab) and Clampfit 8.2 (Axon Instruments). Data are shown as means ± SEM. Statistical data analysis was assessed with Student's *t* test for simple comparisons and one-way ANOVA followed by Tukey's test for multiple comparisons; differences at $P < 0.05$ were considered statistically significant.

RESULTS

Clinical background

The patient (proband) was diagnosed as a newborn with extreme prolongation of the QT interval on the surface electrocardiography (QTc of ∼825 ms) and experienced multiple episodes of ventricular arrhythmia

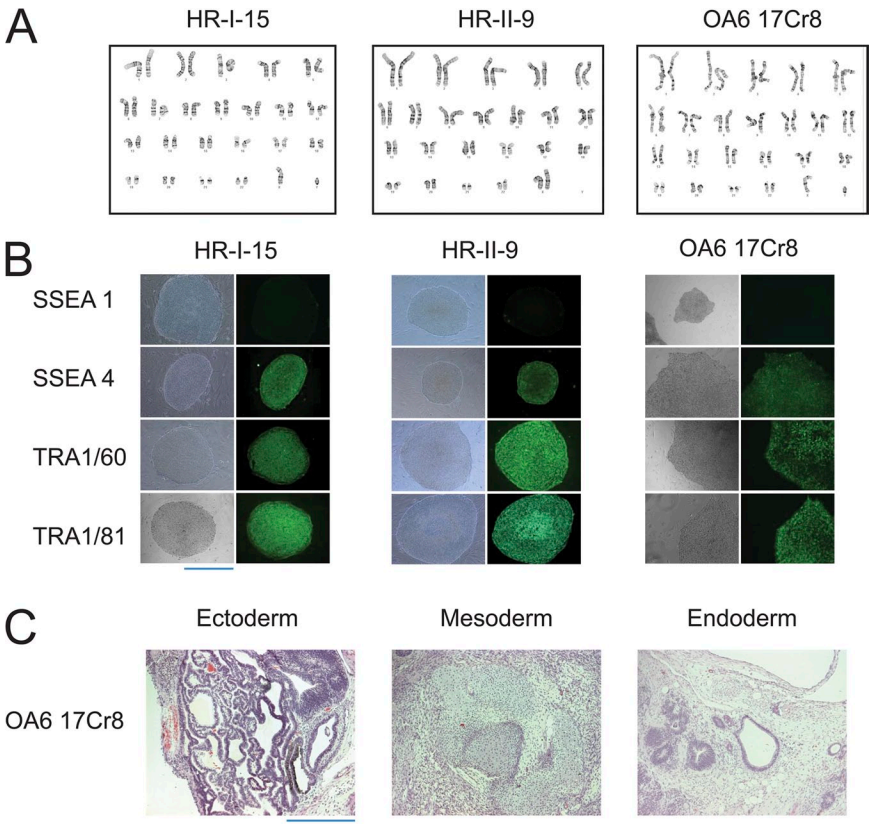

Figure 2. Characterization of iPSC clones from each family member. (A) Karyotype in one clone from each family individual (father, HR-I-15; mother, HR-II-9; proband, OA6 17Cr8). (B) Expression of pluripotency markers in one clone from each family individual (father, HR-I-15; mother, HR-II-9; proband, OA6 17Cr8). (C) Teratoma assay indicated trilineage in vivo differentiation of the proband iPSC clone (OA6 17Cr8). Bars, 200 μm.

called Torsades de pointe. He was found to be heterozygous for a de novo *SCN5A* mutation, F1473C, in the heart $Na_v1.5$ Na^+ channel inactivation gate and for a common polymorphism (K897T) in the hERG channel (*KCNH2*; Fig. 1 A; Bankston et al., 2007b). Neither parent was found to carry the Na^+ channel mutation, but the mother was homozygous for the hERG polymorphism (Fig. 1 A, KCNH2_K897T$^{+/+}$). As a newborn, antiarrhythmic drugs provided mixed results with respect to arrhythmia control; the best control was with mexiletine at higher doses (~6 mg/kg/dose), although the patient continued to have one to five short episodes of ventricular arrhythmia each day (Silver et al., 2009). As a result, a dual chamber implantable cardioverter defibrillator (ICD)/pacemaker was implanted epicardially to help reduce the number of arrhythmias experienced by the patient. Heterologous expression of mutant Na^+ channels in mammalian (HEK293) cells identified a severe defect in inactivation and illustrated the utility of Na^+ channel blockers to correct the mutation-induced channel dysfunction (Bankston et al., 2007b). The contribution of the *KCNH2* polymorphism to the disease phenotype and pro- and anti-arrhythmic drug effects was unknown despite studies suggesting a causal link between this polymorphism and arrhythmia (Bezzina et al., 2003; Paavonen et al., 2003; Anson et al., 2004; Crotti et al., 2005; Rhodes et al., 2008; Sinner et al., 2008). At the start of the present study, the patient was 4 yr old and was maintained on ~24 mg/kg/d mexiletine (divided into every 6–8-h regimen), which is an approximately three to four times higher dose than what is typically used for LQT-3 patients (Ruan et al., 2007), in addition to 5–6 mg/kg/d propranolol and atrial pacing kept at a moderate rate of 80 beats per minute (bpm). Although this regimen improved the patient's condition, it provided an incomplete control of his arrhythmia, as multiple episodes of arrhythmia were still detected daily by his ICD, and numerous shocks by the ICD were required to terminate sustained arrhythmic events (Fig. 1 B). Attempts at increasing mexiletine were limited by the development of frequent seizures associated with only modest fever, suggesting a very narrow therapeutic range for this individual.

Na^+ channel activity in iPSC-CMs

To understand the limitations of this therapeutic approach and the complications of high dose mexiletine therapy, we studied the effects of the drug in iPSC-CMs derived from members of this LQTS family (Sommer et al., 2009; Somers et al., 2010). This approach enabled us to determine channel activity and pharmacology within a genetically correct cardiac background of the patient. First, we generated multiple iPSC clones from dermal fibroblasts of each family member by using the polycistronic reprogramming lentiviral vector (see Materials and methods), hSTEMCCA-loxP (see Materials and methods section Human fibroblast reprogramming . . .). The resulting iPSC clones exhibited a normal karyotype

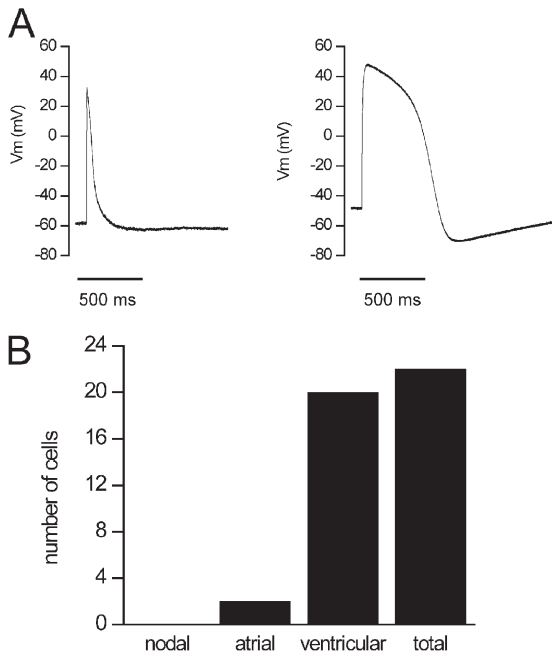

Figure 3. Action potential phenotypes in iPSC-CMs. (A) In a total of 22 cells, 2 different types of action potentials were recorded: atrial-like (left; mean of two cells) and ventricular-like (right; mean of 20 cells). Action potentials were elicited with 3-ms suprathreshold stimuli at 0.2 Hz. (B) Distribution of CMs according to their action potential phenotype: out of 22 cells, 2 cells were atrial-like and 20 cells were ventricular-like.

(Fig. 2 A), expressed stem cell markers (Fig. 2 B), and displayed functional pluripotency in teratoma assays (Fig. 2 C). These iPSC clones were differentiated into CMs (as described in Materials and methods) and then were characterized in patch-clamp experiments.

Current clamp showed that iPSC-CMs from all clones were predominantly characterized by what has been referred to as ventricular-like action potentials when paced with suprathreshold current pulses, and we detected the same distribution of action potential waveforms in the iPSC-CMs as we reported previously in human embryonic stem cells (hESCs) derived using the same procedures (Fig. 3; Wang et al., 2011). The relatively depolarized diastolic membrane potentials recorded in these myocytes at this embryonic developmental stage inactivate sodium channels and consequently minimize contributions of sodium channel activity to action potentials (apparent rapid upstrokes in these recordings reflect artifacts of the current pulse stimuli). As such, current clamp action potential recordings in these cells are not physiologically relevant, and thus we focused our studies on voltage-clamp techniques that allowed us to measure ion channel activity directly.

We first investigated Na^+ channel activity in cells isolated from multiple clones of each family member and found dysfunctional inactivation in cells from all clones from the proband, but not from any clones of either parent. Imposing voltage-clamp waveforms of adult ventricular muscle action potentials clearly revealed the pathophysiological contribution of mutation increase noninactivating or I_{NaL} current apparent in cells from the proband (Fig. 4 B), but not from either parent (Fig. 4 A). We then used square wave voltage-clamp protocols designed to reveal critical biophysical properties of these channels in multiple iPSC clones of both parents and the proband (Fig. 5). We focused on Na^+ channel biophysical properties principally related to channel inactivation because the F1473C mutation had been found to alter Na^+ channel inactivation in heterologous expression studies in HEK293 cells (Bankston et al., 2007b). First, comparison of the biophysical properties of all clones studied from either parent indicated remarkable similarity to properties of Na^+ channels measured in CMs derived from hESCs (hESC-CMs; Satin et al., 2004), validating the use of iPSC-CMs in the measurement of Na^+ channel activity. Second, dysfunction in Na^+ channel gating was clearly detected in all clones from the proband. A mutation-dependent increase in I_{NaL} was detected in all three clones from the proband and none of the parents' clones (Fig. 5, A and B; and Table 1).

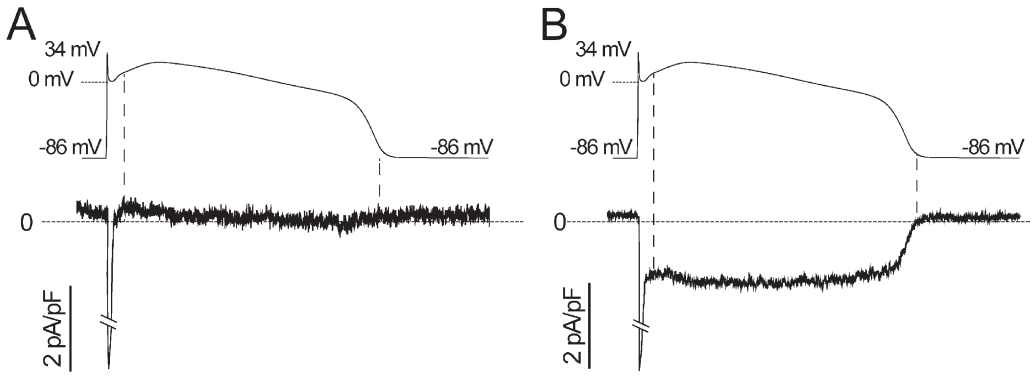

Figure 4. Na^+ channel currents in response to adult ventricular action potential waveforms. (A and B) Adult ventricular action potential waveforms were computed (ten Tusscher et al., 2004) and applied as command waveforms in whole-cell voltage-clamp mode on iPSC-CMs from father (A) and proband (B) using recording solutions to reveal Na^+ channel currents. Mexiletine-dissected Na^+ channel currents are shown, averaged for four (A) and five (B) cells.

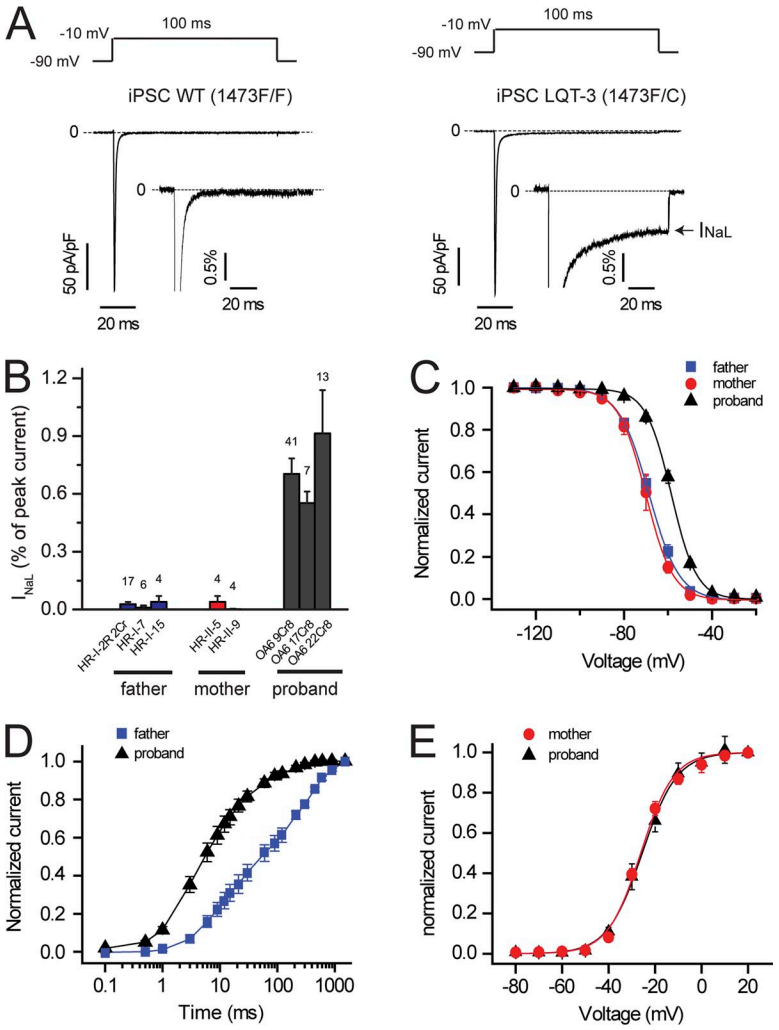

Figure 5. Biophysical properties of Na^+ channels in iPSC-CMs. (A) TTX (50 µM)-sensitive averaged Na^+ current traces recorded from father (WT, $n = 27$, three clones; left) and proband (LQT-3, $n = 41$, clone OA6 9Cr8; right) iPSC-CMs at −10 mV (100-ms pulses at 0.2 Hz from a −90-mV holding potential). Dashed lines, zero current. (insets) I_{Na} normalized to peak current reveal the presence of I_{Na} late current (I_{NaL}; arrow) in LQT-3 but not in WT iPSC-CMs. (B) Percentage of I_{NaL} with respect to peak current measured in three clones from the father, two clones from the mother, and three clones from the proband. (All three LQT-3 clones are $P < 0.01$ vs. each WT clone). The number of cells tested is indicated above each bar. (C) Steady-state availability in LQT-3 (proband, $n = 27$, averaged from two clones) and WT iPSC-CMs (father, $n = 23$, averaged from three clones; mother, $n = 3$, one clone; both are $P < 0.001$ vs. LQT-3). For each individual, data obtained from each clone are detailed in Table 1. (D) Recovery from inactivation in LQT-3 (proband, $n = 6$, clone OA6 9Cr8) and WT iPSC-CMs (father, $n = 4$, clone HR-I-2R 2Cr). Half-time in WT iPSC-CMs is $P < 0.01$ versus LQT-3. (E) Activation curve in LQT-3 (proband, $n = 3$, clone OA6 9Cr8) and WT iPSC-CMs (mother, $n = 3$, clone HR-II-9). $V_{1/2}$ in WT iPSC-CMs is not significantly different from LQT-3. Data are shown as means ± SEM.

Steady-state availability (inactivation) of Na^+ channels in the proband's iPSC-CMs was right shifted compared with channels recorded in the parents' iPSC-CMs (Fig. 5 C and Table 1), whereas activation curves were not changed (Fig. 5 E and Table 1). In addition, Na^+ channel recovery from inactivation in the proband's iPSC-CMs was significantly faster than in WT cells (Fig. 5 D and Table 1). Altogether, these mutation-induced defects in Na^+ channel inactivation (increased I_{NaL}, right-shifted steady-state channel availability, and faster recovery from inactivation), measured for this mutation for the first time in iPSC-CMs derived from the proband, are known to contribute markedly to LQT-3 arrhythmia risk (Clancy and Rudy, 1999; Sampson et al., 2010) and thus provide a mechanistic explanation for the proband's clinical phenotype.

hERG channel activity in iPSC-CMs

As the proband was heterozygous for T897 and K897 hERG and each parent was homozygous for each of these variants, and this channel is the unintended target of many drugs that cause drug-induced arrhythmias (Mitcheson et al., 2005), we next tested for the presence and biophysical properties of these channels in iPSC-CMs. We also compared these results with previously measured hERG activity in hESC-CMs (Wang et al., 2011). hERG channel activity (I_{Kr}) was readily detected as E4031-sensitive current (Fig. 6 A; Rhodes et al., 2008; Sinner et al., 2008) with hallmark rectification in all clones from each family member, as can be seen in the current traces as well as the I-V curves illustrated in the figure (Fig. 6 B). No significant difference in I_{Kr} properties, neither rectification that is seen in the I-V curves (Fig. 6 B) nor in the voltage dependence of activation (Fig. 6, C and D), was observed among all family members and all clones. Importantly, the properties of hERG channels recorded in the iPSC-CMs were remarkably similar to those measured in hESC-CMs that had been differentiated using the same protocols with no significant differences between I_{Kr} properties in hESC-CMs (Wang et al., 2011) and I_{Kr} in any of the iPSC-CM lines (Fig. 6). Thus, we concluded that the iPSC-CMs faithfully express this important cardiac K^+ channel and that there was no impact of the *KCNH2* polymorphism on the baseline biophysical properties

TABLE 1

Biophysical properties of I_{Na} in parents' (WT, 1473F/F) and proband's (LQT-3, 1473F/C) iPSC-CMs

Na^+ channel biophysical properties	WT	LQT-3
I_{NaL} (%)	0.02 ± 0.01 (n = 17, HR-I-2R 2Cr) 0.01 ± 0.01 (n = 6, HR-I-7) 0.04 ± 0.03 (n = 4, HR-I-15) 0.04 ± 0.03 (n = 4, HR-II-5) 0.002 ± 0.002 (n = 4, HR-II-9)	0.71 ± 0.08 (n = 41, OA6 9Cr8)[a] 0.55 ± 0.06 (n = 7, OA6 17Cr8)[a] 0.91 ± 0.22 (n = 13, OA6 22Cr8)[a]
Steady-state inactivation ($V_{1/2}$) (mV)	−68.5 ± 1.7 (n = 13, HR-I-2R 2Cr) −68.9 ± 0.9 (n = 6, HR-I-7) −69.5 ± 2.1 (n = 4, HR-I-15) −70.3 ± 1.7 (n = 3, HR-II-9)	−58.4 ± 0.8 (n = 21, OA6 9Cr8)[a] −59.8 ± 1.4 (n = 6, OA6 17Cr8)[a]
Recovery from inactivation ($t_{1/2}$) (ms)	60.4 ± 14.7 (n = 4, HR-I-2R 2Cr)	6.14 ± 1.2 (n = 6, OA6 9Cr8)[a]
Activation ($V_{1/2}$) (mV)	−25.5 ± 0.3 (n = 3, HR-II-9)	−26.1 ± 0.5 (n = 3, OA6 9Cr8)

I_{Na} late current (I_{NaL}) is expressed as a percentage of I_{Na} peak current. $V_{1/2}$ (in millivolts) indicates the midpoint of steady-state inactivation and activation as determined by fitting data with the Boltzmann equation. $t_{1/2}$ (in milliseconds) is the time for half of the channels to recover from inactivation. Values are reported as means ± SEM. Indicated in parentheses are the number of cells tested (n) and clone names (father, HR-I-2R 2Cr, HR-I-7, and HR-I-15; mother, HR-II-5 and HR-II-9; proband, OA6 9Cr8, OA6 17Cr8, and OA6 22Cr8). Statistical significance was determined with an unpaired Student's t test. With the exception of activation midpoint, all data measured in LQT-3 iPSC-CMs were significantly different from the corresponding data obtained in WT cells. Data obtained from different clones within each group (WT or LQT-3) are not significantly different from each other.
[a]$P < 0.05$.

of hERG channels in these cells. This implies that the Na^+ channel lesion is the primary defect underlying the electrophysiological pathology of the proband.

Molecular pharmacology of mexiletine in iPSC-CMs: Impact on sodium and potassium channels

Having established that the Na^+ channel mutation F1473C is primarily responsible for the prolonged QT interval in the patient, we next investigated the effects of mexiletine on sodium channels in the iPSC-CMs. We chose mexiletine because, to date, this has been the most effective drug in controlling the proband's arrhythmias, and we focused on a high mexiletine concentration both because of the high dose clinical regimen and because the biophysical consequences of the F1473C mutation (right-shifted channel availability) are known

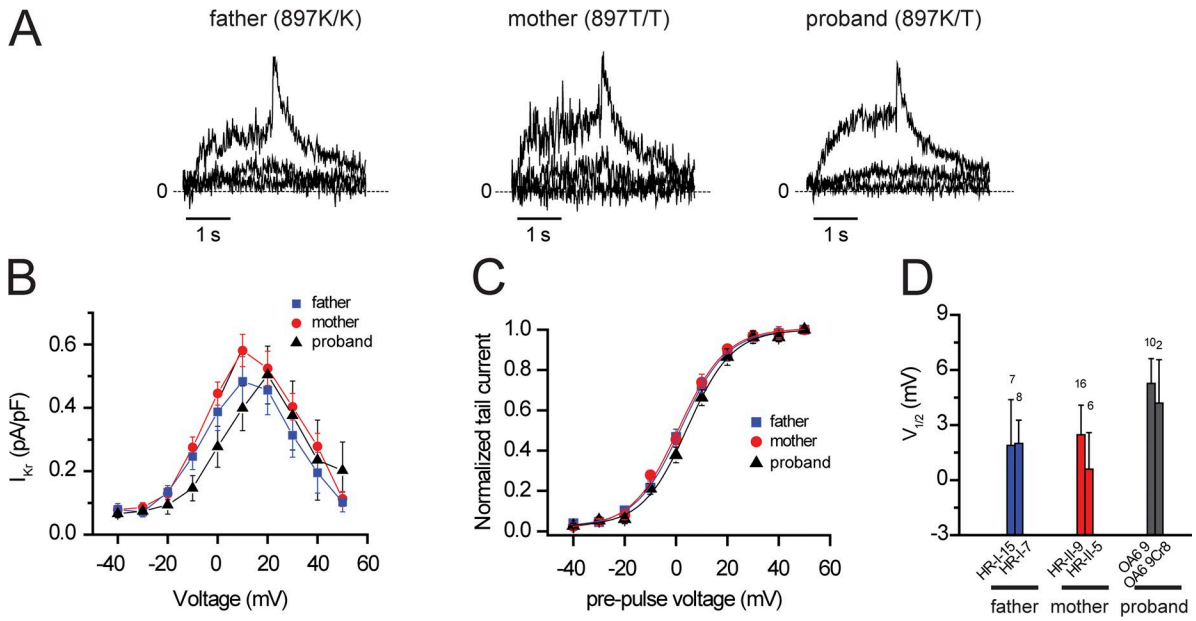

Figure 6. hERG K897T polymorphism does not alter biophysical properties of hERG channels in iPSC-CMs. (A) I_{Kr} currents recorded from father (897K/K), mother (897T/T), and proband (897K/T) iPSC-CMs during 2-s pulses (0.1 Hz) to −40, −10, and 20 mV and for 2 s after return to a −40-mV holding potential. Dashed lines, zero current. (B and C) Current versus test pulse voltage. (B) Current measured at 2 s during test pulse (n = 4–15). (C) Normalized tail current measured at −40 mV (n = 12–22). (D) Bar graph summary showing I_{Kr} midpoint of activation ($V_{1/2}$) for each clone tested and calculated from a Boltzmann fit of normalized tail current. Data are shown as means ± SEM.

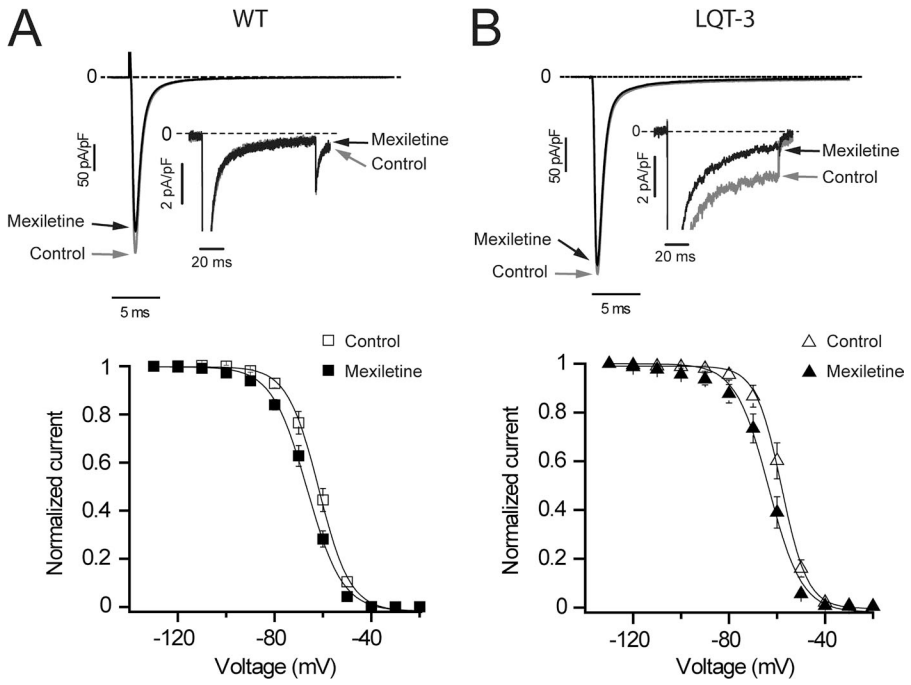

Figure 7. Mexiletine corrects F1473C-altered Na^+ channel inactivation. (A and B, top) Averaged I_{Na} current traces recorded at −10 mV (100-ms pulses applied at 0.2 Hz from a −90-mV holding potential) in father (A; WT, $n = 5$, clone HR-I-2R 2Cr) and proband (B; LQT-3, $n = 18$, clone OA6 9Cr8) iPSC-CMs in control conditions (gray traces and arrows) and in the presence of 50 µM mexiletine (black traces and arrows) at low and high (insets) gain. (insets) I_{Na} at high gain shows the absence of mexiletine-sensitive I_{NaL} in father's iPSC-CMs (A) but reveals the presence of I_{NaL} in LQT-3 iPSC-CMs, which was significantly blocked by 50 µM mexiletine (B, arrow). (A and B, bottom) Steady-state availability in the absence (open symbols) and presence (closed symbols) of 50 µM mexiletine in WT (A; $n = 5$, clone HR-I-2R 2Cr) and LQT-3 (B; $n = 8$, clone OA6 9Cr8) cells. Data are shown as means ± SEM.

to reduce the relative efficacy of mexiletine and other sodium channel blockers (Liu et al., 2003; Ruan et al., 2009). We initially studied drug actions using a fixed pulse frequency of 0.2 Hz and focused on pharmacological modulation of three important channel properties: depolarization-induced peak (initial) current ($I_{Na\,peak}$); late current (I_{NaL}); and the voltage dependence of steady-state inactivation (channel availability; $V_{1/2}$). $I_{Na\,peak}$ is critical for successful conduction in the heart, and thus its inhibition would be detrimental. Fig. 7 compares the effects of mexiletine on Na^+ channel currents from one of the parent's (Fig. 7 A, WT channels) and the proband's (Fig. 7 B) iPSC-CMs. Recordings are illustrated at low and high (Fig. 7, A and B, insets) gains. Low gain recordings were used to determine the effects of mexiletine on $I_{Na\,peak}$, and high gain records were used for I_{NaL}. I_{NaL} is inhibited roughly fourfold more than $I_{Na\,peak}$ in proband's iPSC-CMs (59.1 ± 1.1% block of $I_{Na\,peak}$ vs. 13.5 ± 0.8% block of I_{NaL}; $n = 18$, $P < 0.001$). Note that there is no measureable I_{NaL} for WT channels (Fig. 7 A, top). In addition, we also found that there was no difference in mexiletine block of $I_{Na\,peak}$ in F1473C (see aforementioned data) and WT (14.5 ± 1.9%; $n = 5$) iPSC-CMs. Mexiletine causes a negative shift in steady-state availability for iPSC-CMs from WT cells ($V_{1/2}$ = −66.8 ± 0.9 mV in control vs. $V_{1/2}$ = −71.5 ± 0.8 mV with mexiletine; $n = 5$, $P < 0.05$; Fig. 7 A, bottom) and iPSC-CMs from the proband ($V_{1/2}$ = −58.5 ± 1.6 mV in control vs. $V_{1/2}$ = −64.1 ± 1.9 mV with mexiletine; $n = 8$, $P < 0.05$; Fig. 7 B, bottom). In the case of proband iPSC-CMs, the drug-induced shift rescues inactivation voltage dependence of drug-free iPSC-CM Na^+ channels from the parents (compare closed symbols in Fig. 7 B with open symbols in Fig. 7 A). The results from these experiments provide evidence that mexiletine interacts with Na^+ channels in iPSC-CMs derived from the proband in a manner that would predict anti-arrhythmic actions in the patient, particularly at high drug concentrations because late current is preferentially targeted over peak current, and steady-state inactivation voltage dependence of WT channels is rescued.

Because the iPSC-CMS also express hERG variants that critically contribute to control of QT intervals in the patient and his parents, we also tested for possible mexiletine modulation of current through hERG channels (I_{Kr}) in the iPSC-CMs and focused on possible differences in drug response between hERG variants that differ between the proband and both parents. We found mexiletine inhibits I_{Kr} in cells from both the father (897K/K) and proband (897K/T; Fig. 8 A) with no significant impact of the K897T polymorphism on mexiletine block (Fig. 8 B). Thus, high dose mexiletine has a limited therapeutic dose range, in part because of hERG block that is independent of the K897T polymorphism. For the dosage required for therapeutic block of the I_{NaL} in the proband, concomitant block of hERG limits the ability of mexiletine to fully correct the repolarization defect.

Molecular basis of alternative clinical strategy: Pacing versus the addition of a second drug, flecainide

Because high mexiletine doses were not controlling arrhythmic episodes and our data revealed limitations because of interactions of mexiletine with hERG channels, we investigated alternative strategies to control I_{NaL} in the iPSC-CMs: changes in pacing rate as well as the

impact of adding a second Na^+ channel blocker, flecainide, two clinical options frequently used empirically to treat LQTS-3. We first studied the effect of pulse frequency (heart rate) on I_{NaL} in iPSC-CMs from the proband and parents because for some (Clancy et al., 2002), but not all, LQT-3 (Bankston et al., 2007a) mutants, heart rate (pulse frequency) alone can be a potent modifier of I_{NaL} and late current block by drugs such as mexiletine, and flecainide is use dependent and increases with increased stimulation rate (Moreno et al., 2011). We found I_{NaL} expressed in proband iPSC-CMs was very sensitive to the stimulation rate. Even in the absence of drug, increasing the pulse rate from 0.2 to 1.6 Hz resulted in a 50% decrease in I_{NaL}, and when mexiletine was added, I_{NaL} was reduced further to <15% of drug-free values recorded at the slower pulse rate (Fig. 9, A and B). This improved I_{NaL} block at the higher pulse rate was accompanied by only modest reduction in $I_{Na\ peak}$, ensuring minimal impact on impulse conduction. We found that addition of the second drug, flecainide, had no significant further increase in I_{NaL} block at the higher pulse frequency but further reduced $I_{Na\ peak}$ (Fig. 9 B), predicting little clinical benefit by the addition of the second Na^+ channel blocker. The rate-dependent increase in mexiletine reduction of I_{NaL} was not accompanied by changes in mexiletine I_{Kr} block, but further addition of flecainide more than doubled pro-arrhythmic I_{Kr} inhibition (Fig. 9, C and D). These results, taken together, suggested that the combination drug therapy would not provide additional clinical benefit but was accompanied by potential clinical risk as a result of potentiated I_{Kr} block and suggested that arrhythmogenic consequences of the F1473C mutation would be better controlled at faster heart rates.

DISCUSSION

This study illustrates integration of basic molecular and cellular experiments using iPSCs to suggest therapeutic approaches to manage a rare disease, LQT-3, and demonstrates the importance and potential of iPSC-CMs as a platform for these investigations. The distinct properties of iPSC-CMs derived from the proband compared with those derived from the parents reinforce the utility of these cells in detecting patient-specific channel defects and hence improve potential approaches to manage dysfunctional channel activity. Studies in the iPSC-CMs eliminated a role of the common K897T polymorphism in the response of the patient to anti-arrhythmic drug therapies, a particularly important finding because heterologous expression studies have reported differing effects of this variant on channel activity (Bezzina et al., 2003; Paavonen et al., 2003; Anson et al., 2004; Crotti et al., 2005; Rhodes et al., 2008; Sinner et al., 2008).

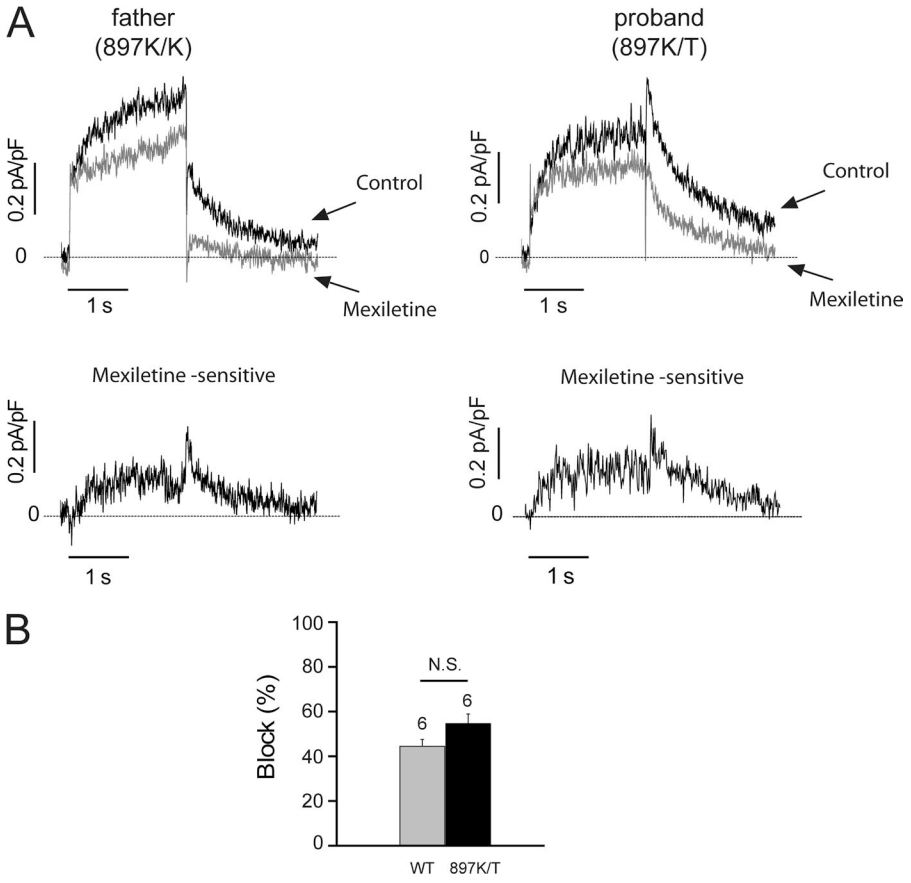

Figure 8. Mexiletine blocks I_{Kr} channels. (A, top) I_{Kr} current traces recorded in father and proband iPSC-CMs during a 2-s depolarizing test pulse to 30 mV followed by a 2-s repolarizing pulse to −40 mV (holding potential was −40 mV) at 0.1 Hz in control conditions (black traces and arrows) and in the presence of 50 µM mexiletine (gray traces and arrows). 30 µM chromanol 293B was added to block I_{Ks}. (bottom) Mexiletine (50 µM)-sensitive potassium currents in iPSC-CMs subtracted from the top recordings. Dashed lines, zero current. (B) 50 µM mexiletine significantly blocked I_{Kr} tail current at −40 mV in iPSC-CMs from the father (WT = 897K/K, $P < 0.05$ vs. control) and proband (897K/T, $P < 0.05$ vs. control). Data are shown as means ± SEM.

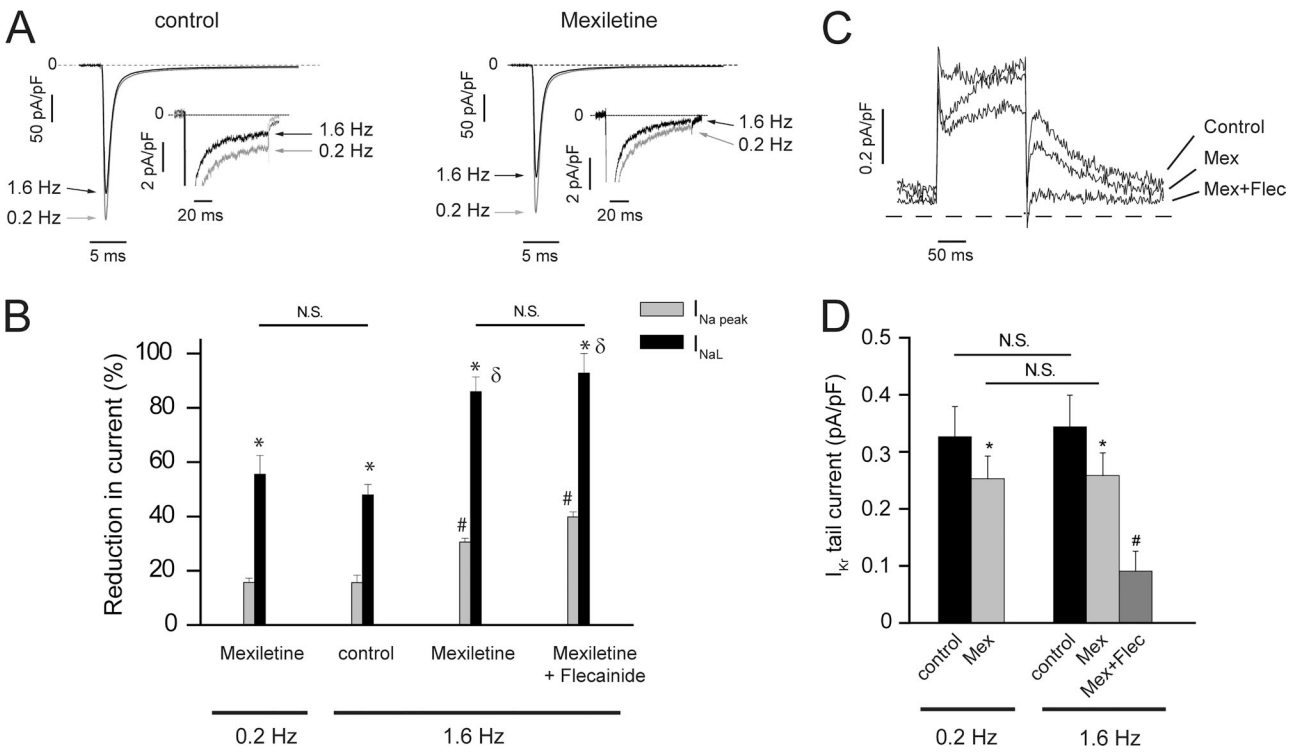

Figure 9. Impact of stimulation frequency on I_{NaL} and I_{Kr} in the absence and presence of drugs. (A) Averaged sodium current traces recorded at −10 mV (100-ms pulses applied from a −90-mV holding potential) in LQT-3 iPSC-CMs in control conditions (left; $n = 5$) and in the presence of 50 µM mexiletine (right; $n = 5$) at 0.2 Hz (gray traces and arrows) and at 1.6 Hz (black traces and arrows) at low and high (insets) gain. Dashed lines, zero current. (B) Percent block of I_{Na} peak current ($I_{Na\ peak}$) and I_{Na} late current (I_{NaL}) at 0.2 and 1.6 Hz by 50 µM mexiletine alone ($n = 6$) and 50 µM mexiletine plus 5 µM flecainide ($n = 3$). One-way ANOVA followed by Tukey's test: *, $P < 0.01$ versus paired $I_{Na\ peak}$; #, $P < 0.01$ versus $I_{Na\ peak}$ at 0.2 Hz in the presence of mexiletine; δ, $P < 0.01$ versus I_{NaL} at 0.2 Hz in the presence of mexiletine. (C) Block of I_{Kr} channels by 50 µM mexiletine (Mex) and 5 µM flecainide (Flec) at 1.6 Hz in WT iPSC-CMs depolarized to 30 mV for 200 ms, from a holding potential of −40 mV, and repolarized at −40 mV for 200 ms. (D) Change in I_{Kr} tail current density measured at −40 mV after 200-ms test pulses at 30 mV in control condition (at 0.2 and 1.6 Hz), in the presence of 50 µM mexiletine and after the addition of 5 µM flecainide. *, $P < 0.05$ versus paired control; #, $P < 0.05$ versus mexiletine at 1.6 Hz. Data are shown as means ± SEM.

The results indicated that the high dose mexiletine regimen initially used to treat the patient was limited by a balance of anti-arrhythmic drug block of I_{NaL} and pro-arrhythmic block of I_{Kr}. This suggested that control of dysfunctional I_{NaL} by mexiletine alone, perhaps at lower concentrations but when applied in concert with higher pacing rates, might be as effective, and perhaps safer, than multidrug therapies at lower heart rates. Consistent with these in vitro predictions, to date the most effective control of arrhythmia burden in the proband has been achieved by increasing atrial pacing via the implanted ICD from 80 bpm to 100 bpm and by mexiletine treatment at a slightly reduced dosage and without a second Na^+ channel blocker. Mechanistically, this is consistent with the established mechanism underlying increased late current in LQT-3: an increased bursting mode of gating. As has been shown with single-channel recordings for numerous LQT-3 mutant channels, the modal shift to bursting is dependent on the time spent in the closed state, which occurs between beats at the diastolic potential, making the disorder more pronounced at a slow heart rate (Clancy and Rudy, 1999; Clancy et al., 2002). Here, we observe a very pronounced rate dependence of disease-causing late current that is consistent with this gating scheme and, in addition, an overall slowing of inactivation recovery kinetics measured in iPSC-CMs compared with previous measurements in HEK293 cells (Bankston et al., 2007b), that, taken together, exacerbate the role of rate in the patient phenotype and provide a mechanistic channel defect explanation for the efficacy of a combined pacing and pharmacological approach to treatment. Altogether, the results of our study strongly support consideration of in vitro iPSC experiments as a new method for optimization of therapy for LQTS.

We thank the patient and family for their generous contribution.

This work was supported by New York State Stem Cell Program (NYSTEM) grant N09G125 (to R.S. Kass, G. Keller, and D.N. Kotton) and New York Stem Cell Foundation grant CU10-0553 (to K. Wang).

Edward N. Pugh Jr. served as editor.

Submitted: 21 September 2012
Accepted: 16 November 2012

REFERENCES

An, R.H., R. Bangalore, S.Z. Rosero, and R.S. Kass. 1996. Lidocaine block of LQT-3 mutant human Na+ channels. *Circ. Res.* 79:103–108. http://dx.doi.org/10.1161/01.RES.79.1.103

Anson, B.D., M.J. Ackerman, D.J. Tester, M.L. Will, B.P. Delisle, C.L. Anderson, and C.T. January. 2004. Molecular and functional characterization of common polymorphisms in HERG (KCNH2) potassium channels. *Am. J. Physiol. Heart Circ. Physiol.* 286:H2434–H2441. http://dx.doi.org/10.1152/ajpheart.00891.2003

Bankston, J.R., K.J. Sampson, S. Kateriya, I.W. Glaaser, D.L. Malito, W.K. Chung, and R.S. Kass. 2007a. A novel LQT-3 mutation disrupts an inactivation gate complex with distinct rate-dependent phenotypic consequences. *Channels (Austin).* 1:273–280.

Bankston, J.R., M. Yue, W. Chung, M. Spyres, R.H. Pass, E. Silver, K.J. Sampson, and R.S. Kass. 2007b. A novel and lethal de novo LQT-3 mutation in a newborn with distinct molecular pharmacology and therapeutic response. *PLoS ONE.* 2:e1258. http://dx.doi.org/10.1371/journal.pone.0001258

Bezzina, C.R., A.O. Verkerk, A. Busjahn, A. Jeron, J. Erdmann, T.T. Koopmann, Z.A. Bhuiyan, R. Wilders, M.M. Mannens, H.L. Tan, et al. 2003. A common polymorphism in KCNH2 (HERG) hastens cardiac repolarization. *Cardiovasc. Res.* 59:27–36. http://dx.doi.org/10.1016/S0008-6363(03)00342-0

Clancy, C.E., and Y. Rudy. 1999. Linking a genetic defect to its cellular phenotype in a cardiac arrhythmia. *Nature.* 400:566–569. http://dx.doi.org/10.1038/23034

Clancy, C.E., M. Tateyama, and R.S. Kass. 2002. Insights into the molecular mechanisms of bradycardia-triggered arrhythmias in long QT-3 syndrome. *J. Clin. Invest.* 110:1251–1262.

Crotti, L., A.L. Lundquist, R. Insolia, M. Pedrazzini, C. Ferrandi, G.M. De Ferrari, A. Vicentini, P. Yang, D.M. Roden, A.L. George Jr., and P.J. Schwartz. 2005. KCNH2-K897T is a genetic modifier of latent congenital long-QT syndrome. *Circulation.* 112:1251–1258. http://dx.doi.org/10.1161/CIRCULATIONAHA.105.549071

Gnecchi, M., and P.J. Schwartz. 2012. The unstoppable attraction for induced pluripotent stem cells: are they the magic bullet for modeling inherited arrhythmogenic diseases? *J. Am. Coll. Cardiol.* 60:1001–1004. http://dx.doi.org/10.1016/j.jacc.2012.04.019

Itoh, H., W. Shimizu, K. Hayashi, K. Yamagata, T. Sakaguchi, S. Ohno, T. Makiyama, M. Akao, T. Ai, T. Noda, et al. 2010. Long QT syndrome with compound mutations is associated with a more severe phenotype: a Japanese multicenter study. *Heart Rhythm.* 7:1411–1418. http://dx.doi.org/10.1016/j.hrthm.2010.06.013

Itzhaki, I., L. Maizels, I. Huber, L. Zwi-Dantsis, O. Caspi, A. Winterstern, O. Feldman, A. Gepstein, G. Arbel, H. Hammerman, et al. 2011. Modelling the long QT syndrome with induced pluripotent stem cells. *Nature.* 471:225–229. http://dx.doi.org/10.1038/nature09747

Jung, C.B., A. Moretti, M. Mederos y Schnitzler, L. Iop, U. Storch, M. Bellin, T. Dorn, S. Ruppenthal, S. Pfeiffer, A. Goedel, et al. 2012. Dantrolene rescues arrhythmogenic RYR2 defect in a patient-specific stem cell model of catecholaminergic polymorphic ventricular tachycardia. *EMBO Mol Med.* 4:180–191. http://dx.doi.org/10.1002/emmm.201100194

Kamp, T.J. 2011. An electrifying iPSC disease model: long QT syndrome type 2 and heart cells in a dish. *Cell Stem Cell.* 8:130–131. http://dx.doi.org/10.1016/j.stem.2011.01.010

Kass, R.S., and A.J. Moss. 2006. Mutation-specific pharmacology of the long QT syndrome. In *Basis and treatment of cardiac arrhythmias.* Handbook of Experimental Pharmacology, Vol. 171. R.S. Kass and C.E. Clancy, editors. Springer-Verlag, Berlin. 287–304.

Kattman, S.J., A.D. Witty, M. Gagliardi, N.C. Dubois, M. Niapour, A. Hotta, J. Ellis, and G. Keller. 2011. Stage-specific optimization of activin/nodal and BMP signaling promotes cardiac differentiation of mouse and human pluripotent stem cell lines. *Cell Stem Cell.* 8:228–240. http://dx.doi.org/10.1016/j.stem.2010.12.008

Kennedy, M., S.L. D'Souza, M. Lynch-Kattman, S. Schwantz, and G. Keller. 2007. Development of the hemangioblast defines the onset of hematopoiesis in human ES cell differentiation cultures. *Blood.* 109:2679–2687.

Liu, H., J. Atkins, and R.S. Kass. 2003. Common molecular determinants of flecainide and lidocaine block of heart Na^+ channels: evidence from experiments with neutral and quaternary flecainide analogues. *J. Gen. Physiol.* 121:199–214. http://dx.doi.org/10.1085/jgp.20028723

Masuda, S., and Y. Hanazono. 2011. Induced pluripotent stem cells in long-QT syndrome. *N. Engl. J. Med.* 364:181; author reply 181–182. http://dx.doi.org/10.1056/NEJMc1012529

Mitcheson, J.S., J. Chen, M. Lin, C. Culberson, and M.C. Sanguinetti. 2000. A structural basis for drug-induced long QT syndrome. *Proc. Natl. Acad. Sci. USA.* 97:12329–12333. http://dx.doi.org/10.1073/pnas.210244497

Mitcheson, J., M. Perry, P. Stansfeld, M.C. Sanguinetti, H. Witchel, and J. Hancox. 2005. Structural determinants for high-affinity block of hERG potassium channels. *Novartis Found. Symp.* 266:136–150; discussion 150–158. http://dx.doi.org/10.1002/047002142X.ch11

Moreno, J.D., Z.I. Zhu, P.C. Yang, J.R. Bankston, M.T. Jeng, C. Kang, L. Wang, J.D. Bayer, D.J. Christini, N.A. Trayanova, et al. 2011. A computational model to predict the effects of class I anti-arrhythmic drugs on ventricular rhythms. *Sci. Transl. Med.* 3:98ra83. http://dx.doi.org/10.1126/scitranslmed.3002588

Moretti, A., M. Bellin, A. Welling, C.B. Jung, J.T. Lam, L. Bott-Flügel, T. Dorn, A. Goedel, C. Höhnke, F. Hofmann, et al. 2010. Patient-specific induced pluripotent stem-cell models for long-QT syndrome. *N. Engl. J. Med.* 363:1397–1409. http://dx.doi.org/10.1056/NEJMoa0908679

Moss, A.J., and R.S. Kass. 2005. Long QT syndrome: from channels to cardiac arrhythmias. *J. Clin. Invest.* 115:2018–2024. http://dx.doi.org/10.1172/JCI25537

Novak, A., L. Barad, N. Zeevi-Levin, R. Shick, R. Shtrichman, A. Lorber, J. Itskovitz-Eldor, and O. Binah. 2012. Cardiomyocytes generated from CPVTD307H patients are arrhythmogenic in response to β-adrenergic stimulation. *J. Cell. Mol. Med.* 16:468–482. http://dx.doi.org/10.1111/j.1582-4934.2011.01476.x

Paavonen, K.J., H. Chapman, P.J. Laitinen, H. Fodstad, K. Piippo, H. Swan, L. Toivonen, M. Viitasalo, K. Kontula, and M. Pasternack. 2003. Functional characterization of the common amino acid 897 polymorphism of the cardiac potassium channel KCNH2 (HERG). *Cardiovasc. Res.* 59:603–611. http://dx.doi.org/10.1016/S0008-6363(03)00458-9

Rhodes, T.E., R.L. Abraham, R.C. Welch, C.G. Vanoye, L. Crotti, M. Arnestad, R. Insolia, M. Pedrazzini, C. Ferrandi, A. Vege, et al. 2008. Cardiac potassium channel dysfunction in sudden infant death syndrome. *J. Mol. Cell. Cardiol.* 44:571–581. http://dx.doi.org/10.1016/j.yjmcc.2007.11.015

Ruan, Y., N. Liu, R. Bloise, C. Napolitano, and S.G. Priori. 2007. Gating properties of SCN5A mutations and the response to mexiletine in long-QT syndrome type 3 patients. *Circulation.* 116:1137–1144. http://dx.doi.org/10.1161/CIRCULATIONAHA.107.707877

Ruan, Y., N. Liu, and S.G. Priori. 2009. Sodium channel mutations and arrhythmias. *Nat. Rev. Cardiol.* 6:337–348. http://dx.doi.org/10.1038/nrcardio.2009.44

Sampson, K.J., V. Iyer, A.R. Marks, and R.S. Kass. 2010. A computational model of Purkinje fibre single cell electrophysiology: implications for the long QT syndrome. *J. Physiol.* 588:2643–2655. http://dx.doi.org/10.1113/jphysiol.2010.187328

Satin, J., I. Kehat, O. Caspi, I. Huber, G. Arbel, I. Itzhaki, J. Magyar, E.A. Schroder, I. Perlman, and L. Gepstein. 2004. Mechanism of spontaneous excitability in human embryonic stem cell derived cardiomyocytes. *J. Physiol.* 559:479–496. http://dx.doi.org/10.1113/jphysiol.2004.068213

Sauer, A.J., A.J. Moss, S. McNitt, D.R. Peterson, W. Zareba, J.L. Robinson, M. Qi, I. Goldenberg, J.B. Hobbs, M.J. Ackerman, et al. 2007. Long QT syndrome in adults. *J. Am. Coll. Cardiol.* 49:329–337. http://dx.doi.org/10.1016/j.jacc.2006.08.057

Schwartz, P.J., S.G. Priori, E.H. Locati, C. Napolitano, F. Cantù, J.A. Towbin, M.T. Keating, H. Hammoude, A.M. Brown, and L.S. Chen. 1995. Long QT syndrome patients with mutations of the SCN5A and HERG genes have differential responses to Na+ channel blockade and to increases in heart rate. Implications for gene-specific therapy. *Circulation.* 92:3381–3386. http://dx.doi.org/10.1161/01.CIR.92.12.3381

Silver, E.S., L. Liberman, W.K. Chung, H.M. Spotnitz, J.M. Chen, M.J. Ackerman, C. Moir, A.J. Hordof, and R.H. Pass. 2009. Long QT syndrome due to a novel mutation in SCN5A: treatment with ICD placement at 1 month and left cardiac sympathetic denervation at 3 months of age. *J. Interv. Card. Electrophysiol.* 26:41–45. http://dx.doi.org/10.1007/s10840-009-9428-1

Sinner, M.F., A. Pfeufer, M. Akyol, B.M. Beckmann, M. Hinterseer, A. Wacker, S. Perz, W. Sauter, T. Illig, M. Näbauer, et al. 2008. The non-synonymous coding IKr-channel variant KCNH2-K897T is associated with atrial fibrillation: results from a systematic candidate gene-based analysis of KCNH2 (HERG). *Eur. Heart J.* 29:907–914. http://dx.doi.org/10.1093/eurheartj/ehm619

Somers, A., J.C. Jean, C.A. Sommer, A. Omari, C.C. Ford, J.A. Mills, L. Ying, A.G. Sommer, J.M. Jean, B.W. Smith, et al. 2010. Generation of transgene-free lung disease-specific human induced pluripotent stem cells using a single excisable lentiviral stem cell cassette. *Stem Cells.* 28:1728–1740. http://dx.doi.org/10.1002/stem.495

Sommer, C.A., M. Stadtfeld, G.J. Murphy, K. Hochedlinger, D.N. Kotton, and G. Mostoslavsky. 2009. Induced pluripotent stem cell generation using a single lentiviral stem cell cassette. *Stem Cells.* 27:543–549. http://dx.doi.org/10.1634/stemcells.2008-1075

ten Tusscher, K.H., D. Noble, P.J. Noble, and A.V. Panfilov. 2004. A model for human ventricular tissue. *Am. J. Physiol. Heart Circ. Physiol.* 286:H1573–H1589. http://dx.doi.org/10.1152/ajpheart.00794.2003

Terrenoire, C., C.E. Clancy, J.W. Cormier, K.J. Sampson, and R.S. Kass. 2005. Autonomic control of cardiac action potentials: role of potassium channel kinetics in response to sympathetic stimulation. *Circ. Res.* 96:e25–e34. http://dx.doi.org/10.1161/01.RES.0000160555.58046.9a

Tiscornia, G., N. Monserrat, and J.C. Izpisua Belmonte. 2011. Modelling long QT syndrome with iPS cells: be still, my beating heart... *Circ. Res.* 108:648–649. http://dx.doi.org/10.1161/RES.0b013e318216f0db

Wang, K., C. Terrenoire, K.J. Sampson, V. Iyer, J.D. Osteen, J. Lu, G. Keller, D.N. Kotton, and R.S. Kass. 2011. Biophysical properties of slow potassium channels in human embryonic stem cell derived cardiomyocytes implicate subunit stoichiometry. *J. Physiol.* 589:6093–6104.

Westenskow, P., I. Splawski, K.W. Timothy, M.T. Keating, and M.C. Sanguinetti. 2004. Compound mutations: a common cause of severe long-QT syndrome. *Circulation.* 109:1834–1841. http://dx.doi.org/10.1161/01.CIR.0000125524.34234.13

Yazawa, M., B. Hsueh, X. Jia, A.M. Pasca, J.A. Bernstein, J. Hallmayer, and R.E. Dolmetsch. 2011. Using induced pluripotent stem cells to investigate cardiac phenotypes in Timothy syndrome. *Nature.* 471:230–234. http://dx.doi.org/10.1038/nature09855

Zhang, H., B. Zou, H. Yu, A. Moretti, X. Wang, W. Yan, J.J. Babcock, M. Bellin, O.B. McManus, G. Tomaselli, et al. 2012. Modulation of hERG potassium channel gating normalizes action potential duration prolonged by dysfunctional KCNQ1 potassium channel. *Proc. Natl. Acad. Sci. USA.* 109:11866–11871. http://dx.doi.org/10.1073/pnas.1205266109